Additional Developments in Atmosphere Revitalization Modeling and Simulation

Robert F. Coker, James C. Knox, Ramona Cummings, Thomas Brooks, and Richard G. Schunk
NASA Marshall Space Flight Center, Huntsville, AL, 35812, USA

NASA's Advanced Exploration Systems (AES) program is developing prototype systems, demonstrating key capabilities, and validating operational concepts for future human missions beyond Earth orbit. These forays beyond the confines of earth's gravity will place unprecedented demands on launch systems. They must launch the supplies needed to sustain a crew over longer periods for exploration missions beyond earth's moon. Thus all spacecraft systems, including those for the separation of metabolic carbon dioxide and water from a crewed vehicle, must be minimized with respect to mass, power, and volume. Emphasis is also placed on system robustness both to minimize replacement parts and ensure crew safety when a quick return to earth is not possible. Current efforts are focused on improving the current state-of-the-art systems utilizing fixed beds of sorbent pellets by evaluating structured sorbents, seeking more robust pelletized sorbents, and examining alternate bed configurations to improve system efficiency and reliability. These development efforts combine testing of sub-scale systems and multi-physics computer simulations to evaluate candidate approaches, select the best performing options, and optimize the configuration of the selected approach. This paper describes the continuing development of atmosphere revitalization models and simulations in support of the Atmosphere Revitalization Recovery and Environmental Monitoring (ARREM) project within the AES program.

Nomenclature

q_{si}	=	saturation capacity in multi-species Toth equation, mol kg^{-1}
m_{0i}	=	multi-species Toth equation parameter
m_{Ti}	=	multi-species Toth equation parameter, K
B_i	=	constant in multi-species Toth equation, K
b_{0i}	=	multi-speciesToth equation parameter, kPa^{-1}
q	=	pellet loading, mol m^{-3}
$\dot{q}$	=	time rate of change of pellet loading, mol m^{-3} s^{-1}
q^*	=	equilibrium pellet loading, mol m^{-3}
c	=	concentration of water vapor, mol m^{-3}
$\dot{c}$	=	time rate of change of water vapor concentration, mol m^{-3} s^{-1}
D_i	=	axial dispersion coefficient, m^2 s^{-1}
$\vec{\mathbf{u}}$	=	fluid (air) velocity
ρ	=	density, kg m^{-3}
C_p	=	heat capacity, J kg^{-1} K^{-1}
T	=	temperature, K
$\dot{T}$	=	time rate of change of temperature, K s^{-1}
T_{bndry}	=	temperature of adjacent boundary material, K
k_m	=	mass transfer coefficient, s^{-1}
$\vec{\mathbf{n}}$	=	unit vector normal to component surface
k	=	thermal conductivity, W m^{-1} K^{-1}
h	=	heat transfer coefficient, W m^{-2} K^{-1}
Q	=	Heating source due to sorption, W m^{-3}
$\partial H_{sorbent}$	=	differential heat of adsorption, kJ mol^{-1}
$\varepsilon_{sorbent}$	=	Porosity in the sorbent beds

ε_0 = centerline porosity in the sorbent beds
C_ε = $1/\varepsilon_0 - 1$
N_ε = 4
R_{wall} = distance to nearest wall, m
$D_{pellets}$ = mean diameter of sorbent pellets, mm
$\kappa_{sorbent}$ = Permeability through the sorbent beds, m^2
ε_{plates} = Porosity in the heat exchanger plates
κ_{plates} = Permeability through the heat exchanger plates, m^2
N = number of holes in each heat exchanger plate
A_{HXhole} = area of one hole in a heat exchanger plate, m^2
A_{plate} = cross-sectional area of an entire heat exchanger plate, m^2
r_{HXhole} = radius of one hole in a heat exchanger plate, m
ARREM = Atmosphere Revitalization Recovery and Environmental Monitoring
AES = Advanced Exploration Systems
SG = Silica Gel
HX = Heat Exchanger
VSA = vacuum swing adsorption
HC = half-cycle (time to purge or hydrate one bed), s
IBD = isothermal bulk desiccant
slpm = standard (1 atm, 0 ºC) liters per minute

I. Introduction

Predictive simulation tools are being developed to reduce the hardware testing requirements of the Atmosphere Revitalization Recovery and Environmental Monitoring (ARREM) project. Although sub-scale testing is required to establish the predictive capability of the simulation, the much greater cost of extensive full-scale testing can be limited to that required for the confirmation of analytical design optimization studies. Non-recurring costs of predictive simulation development are non-trivial. However, once predicative capability is established, geometric reconfiguration of a model is usually straightforward. A predictive simulation capability provides numerous additional benefits. Understanding of complex processes is greatly increased since process conditions (temperature, pressure, concentrations, etc.) may be examined anywhere in the adsorption column. Weaknesses in a prototype design can be readily identified and improvements tested via simulation. Finally, the predictive simulation provides a powerful tool for virtual troubleshooting of deployed flight hardware.

II. Process Design Approach

Adsorption in packed fixed beds of pelletized sorbents is presently the primary means of gas separation for atmosphere revitalization systems. However, structured sorbents are emerging as a new approach to sorbent systems. Structured sorbents are produced as monoliths, with an open structure for airflow, or by fixing sorbents on an inert substrate such as paper-like honeycomb structures or expanded metal sheets. A well designed structured sorbent is not as subject to attrition (e.g., due to fines or dust generation) as a packed bed. Also, by using a thermally conductive substrate, the heat of adsorption can be transferred out of the bed, possibly to the cold desorbing bed if geometry permits. However, structured sorbents must be evaluated to determine their applicability to commercial processes and space flight. It must be shown that, in addition to providing a more robust solution, the resource requirements (i.e., weight, power, volume, etc.) are similar to, if not less than, the state-of-the-art packed bed configuration.

An accurate assessment of structured sorbents and comparison with packed bed designs is desirable; experimental results so far show unanticipated variation in packed bed breakthrough for identical beds held under the same conditions. It is suspected that small packing irregularities can propagate downstream in large beds and impact process efficiency. This indicates a margin of error inherent in packed bed fabrication and thus a likely superiority of structured sorbents for process efficiency and control. This paper discusses modeling results using COMSOL's Multiphysics code for a fixed bed design and a membrane based design, as well as a proof of concept (POC) design based on vacuum swing adsorption (VSA).

For the bulk separation of CO_2 and H_2O, temperature changes due to the heat of adsorption are significant, requiring the simulation of the heat balance equations through both the beds and the housing, as well as the equations for sorption processes and fluid flow. For columns with small tube diameter to pellet diameter ratios, as encountered in internally heated columns, flow channeling along the column wall can have a strong influence on

overall performance. In non-cylindrical flow, the influence is great enough to necessitate the use of 3-D simulations.

III. Isothermal Bulk Desiccant

Figure 1. Sub-scale IBD test setup, with two beds, each with 4 cells.

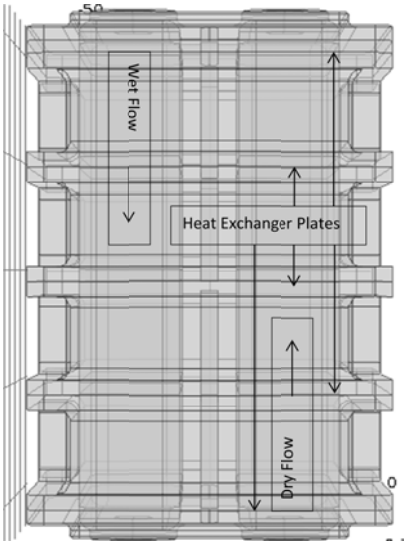

Figure 2. IBD wireframe schematic showing flow paths and HX plates.

A. Description

A water-saving bulk drying stage prior to downstream CO_2 removal processes is under development by NASA. The primary goal is to continuously remove at least 80% and up to 100% of water from a process air stream. Ideally, the bulk dryer will operate without active heating during regeneration to minimize power requirements. This may be accomplished by using the dry CO_2 removal system outlet air to regenerate the bulk dryer via purging. This also returns the captured water back to the cabin atmosphere. Process optimizations such as passive thermal control are of prime interest. Development of a bulk drying stage has focused on a silica gel-based isothermal bulk desiccant (IBD) system with emphasis on evaluating the performance benefits of thermally linking the adsorbing and desorbing beds. The latest IBD prototype is shown in Fig. 1, while a wireframe cutaway is shown in Fig. 2. Every half-cycle (HC), the flow paths switch sides; in this set up, the dry purge flow is always from the bottom and the wet flow is always from the top. Grace Grade 40 Silica Gel (SG) fills the IBD between the heat exchanger (HX) plates to remove water from the air on the wet side, and reintroduces water into the air on the dry side. Aluminum 7075 plates with holes serve as heat exchangers that thermally connect the dry cells to the wet cells. Spring plates, made of the same material and with the same holes as the HX plates, are used, along with fine screen meshes, to hold the SG pellets in place. The IBD is being analyzed to determine if thermal linking can provide substantial efficiency gains. Experimental data will be used to validate the 3-D simulation process so that simulation-driven optimization may be used alongside conventional design methods to perfect a thermally linked desiccant bed design.

B. Models

Initial models of the 2-column 4-cell IBD with HX plates were conducted using the COMSOL Multiphysics code. The physics modules that were applied to the IBD include: Wall Distance, Free and Porous Media Flow, Heat Transfer in Porous Media, Transport of Diluted Species, Heat Transfer in Solids, and Domain ODEs and DAEs (to determine pellet loading). The Wall Distance module was applied in all sorbent bed volumes to determine the distance from every location to the nearest wall, $\boldsymbol{R_{wall}}$. This is used in Eq. (1) to determine the sorbent's local porosity:

$$\epsilon_{sorbent} = \epsilon_0 * \left(1 + C_\epsilon * e^{-N_\epsilon * \frac{R_{wall}}{D_{pellets}}}\right) \quad (1).$$

The local permeability within each cell is found by using the empirical (RG) Eq. (2):

$$\kappa_{sorbent} = \frac{\epsilon_{sorbent}^{5.5} * D_{pellets}^{2}}{5.6} \quad (2).$$

The Free and Porous Media Flow module models the flow based on Navier-Stokes and Brinkman equations while assuming compressible flow; this is applied everywhere there is air flow. The boundary conditions are pressure conditions without viscous stress. The exit pressure is set to match the experiments, while the inlet values are

picked to reproduce the experiment volumetric flow rates of 160 slpm for the purge flow and 190 slpm for the wet flow. The heat exchanger plates are assumed to have the characteristics of porous media in order to relieve the computational burden associated with the fine meshing requirements of a plate with numerous small holes. Note the meshes and spring plates are not included in these models. The porosity of the heat exchanger plates is found using Eq. (3):

$$\epsilon_{plates} = \frac{N * A_{HXhole}}{A_{Plate}} \quad (3),$$

which defines the porosity as being the area of one plate's cross section that air can travel through divided by the total area of the plate's cross section. The permeability of each plate is then determined by Eq. (4):

$$\kappa_{plates} = \frac{(r_{HXhole})^2 * \epsilon_{plates}}{8} \quad (4).$$

Forchheimer drag is added to the model in the sorbent beds and provides a drag term that is proportional to the square of the fluid velocity.

The Heat Transfer in Porous Media module models heat transfer throughout all airflow domains. In the model, the HX plates are separate geometric objects from the chassis, while in the experiments they are one component; thus, the heat transfer between the heat exchanger plates and the IBD chassis is modeled with a large heat transfer coefficient to better resemble conduction through a single piece of metal. The heat gained or lost through sorption is modeled as a heat source which transfers heat to or from the bed at the rate per volume, $\boldsymbol{Q}$, defined in Eq. (5):

$$\boldsymbol{Q} = -\dot{\boldsymbol{q}}(\mathbf{1} - \boldsymbol{\epsilon_{sorbent}})\boldsymbol{\partial H_{sorbent}} \quad (5).$$

The Domain ODEs and DAEs module is applied to determine the loading change with respect to time, $\dot{\boldsymbol{q}}$. The ODE applies the linear driving force (LDF) model and is shown in Eq. (6):

$$\dot{\boldsymbol{q}} = \boldsymbol{k_m}(\boldsymbol{q^*} - \boldsymbol{q}) \quad (6).$$

The saturated equilibrium loading, $\boldsymbol{q^*}$, is temperature and pressure dependent and is determined from the Toth isotherms for silica gel and water vapor. The mass transfer coefficient, $\boldsymbol{k_m}$, is empirically determined from breakthrough experiments.

The Transport of Diluted Species module is used to track the water vapor in the air through the inlet/exit manifolds, HX plates, and beds. Air enters the wet column at a concentration of 0.52 mol m^{-3} and enters the dry column at a concentration of 0.008 mol m^{-3}, corresponding to dew points of 10 ºC and -40 ºC, respectively. All transport comes from convection and diffusion. The diffusion in the air-only manifold regions is isotropic, while diffusion in the heat exchangers is restricted to the direction parallel to the heat exchanger holes, and the diffusion coefficient in the sorbent beds are set to the axial dispersion in the direction of flow and 2/11ths of that value in the other directions. The volumetric rate at which sorption drives the water vapor concentration in the beds is the right-hand-side (RHS) of Eq. (7), the transport equation:

$$\dot{\boldsymbol{c}} + \boldsymbol{\nabla} \cdot (-\mathbf{D_i}\boldsymbol{\nabla}\mathbf{c_i}) + \vec{\mathbf{u}} \cdot \boldsymbol{\nabla}\mathbf{c_i} = \frac{\dot{q}(1-\epsilon_{sorbent})}{\epsilon_{sorbent}} \quad (7).$$

The Heat Transfer in Solids and Heat Transfer in Porous Media modules are used to determine the temperature distribution in the chassis and air-flow regions, respectively. These solve the heat equation as shown in Eq. (8):

$$(\boldsymbol{\rho}\mathbf{c_p})_{\mathbf{eq}}\dot{\boldsymbol{T}} + \boldsymbol{\rho}\mathbf{c_p}\vec{\mathbf{u}} \cdot \boldsymbol{\nabla}\mathbf{T} - \boldsymbol{\nabla} \cdot (\mathbf{k_{eq}}\boldsymbol{\nabla}\mathbf{T}) = \mathbf{Q} \quad (8).$$

The subscript 'eq' refers to volume-weighted average values of the air and sorbent for the porous regions. Note that **Q** outside of the sorbent beds is identically 0. The chassis is insulated, so no heat is transferred to its surroundings. However, between the chassis and the internal domains, the flux boundary condition shown in Eq. (9) is used:

$$-\vec{\mathbf{n}} \cdot (-\mathbf{k}\boldsymbol{\nabla}\mathbf{T}) = \mathbf{h} \cdot (\mathbf{T_{bndry}} - \mathbf{T}) \quad (9).$$

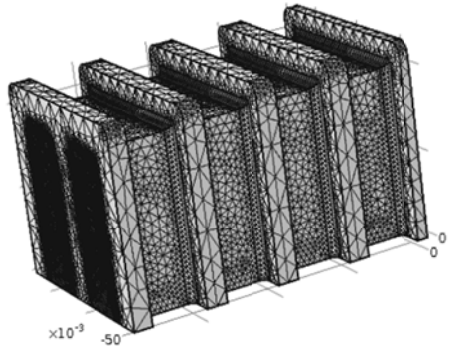

Figure 3. Simplified mesh IBD model.

C. Results and Discussion

Unsurprisingly, initial results of the COMSOL models showed that mesh boundary layers were required on the manifolds, the beds and the HX plate edges to get consistent results with a converged mass flow rate through the IBD. However, with the manifolds in particular, this required too many cells and degrees of freedom to be solvable in practice. Thus, the manifolds were removed, mid-plane symmetry was assumed, and a uniform inlet flow field into the first HX plate was imposed. In addition, consistent with the experimental results, run-time convergence to a quasi-steady state from uniform initial conditions takes ~50 HCs. The simplified mesh model is shown in Fig. 3. Water concentration results along the center of one bed for a 10 minute HC are shown in Fig. 4, illustrating the run-time convergence issue. The lower

curves are for when that bed is experiencing purge flow, while the upper curves are when the bed is experiencing adsorbing flow. Note that time progresses to the upper left and each curve is at the end of a HC. Thus, although the overall bed efficiency, at ~85%, is not changing much with time, internally the bed is adsorbing and desorbing more and more water as time goes on; the last curve is after 33 HCs and a quasi-steady state has clearly not yet been achieved, even though the pellet loading has converged to with 20% of the equilibrium loading. Figure 5 shows the predicted time-integrated sorption efficiency, $1\text{-}P_{vapout}/P_{vapin}$, compared to the measured results. COMSOL is slightly more efficient, probably due to the excess sorbent present in the model due to not including the spring plates. Also, the experiment likely has small inefficiencies, due to imperfect insulation and air leaks, that are not included in the model. For example, the 15 minute HC experiment did not include some bolts that tighten the cells together and thus had a higher pressure loss across the IBD as well as a relatively low efficiency. However, so far the model fails to quantitatively reproduce the temperature and dew point curves, although it gets the trends and shapes correct; a number of possible causes are currently being explored. Even given these differences, the predictive capability of COMSOL for the IBD efficiency seems adequate to aid in future design.

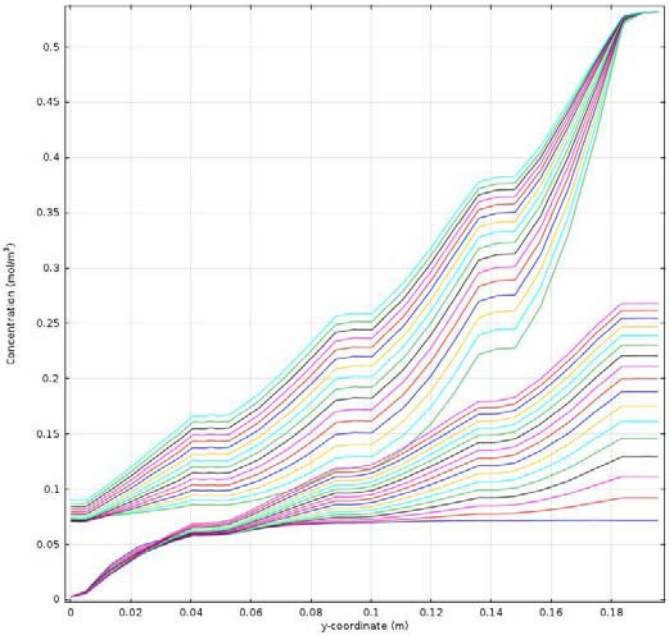

Figure 4. Concentration evolution for the IBD COMSOL reduced model.

IV. Microlith

D. Description

Precision Combustion, Inc. (PCI), via NASA-sponsored projects, has been developing regenerable Microlith®- based adsorber modules for the separation of air constituents such as humidity, CO_2, and trace contaminants to function in either closed or open loop operations. The Microlith® adsorbers use a patented technology developed by PCI to coat expanded metal with zeolite sorbent crystals to produce a structured sorbent. An advantage of this configuration is that it can be thermally regenerated by passing a current through the electrically-resistive expanded metal. Previous developmental work has focused on testing individual Microlith®-based adsorber modules for residual humidity removal, trace contaminant removal, and CO_2 removal. The most recent developmental work evaluated the integrated operation of the residual H_2O removal and CO_2 removal adsorber modules. The adsorber design concept is shown in Fig. 22 (Perry et. al. 2009). The operation of the concept is sketched out in Fig. 23.

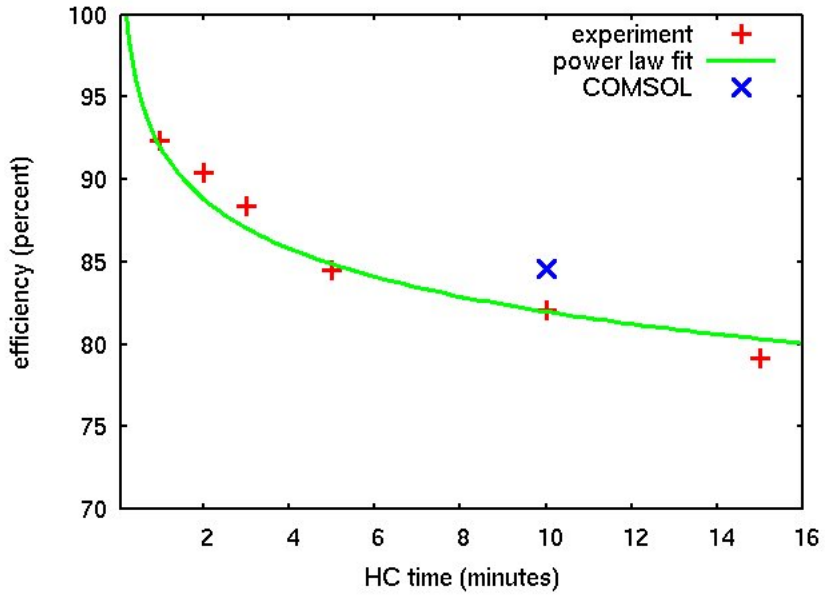

Figure 5. Efficiency predicted by COMSOL (blue) and from experiments (red), along with a power law fit that goes as $HC^{(-1/20)}$.

The full scale water Microlith® "Jelly Roll" was previously modeled for comparison with exit axial velocity measurements. The COMSOL Multiphysics modeling package, with porous media equations and axisymmetric geometry, was used. Inspection of model results helped to identify a probable bypass flow of the sorbent bed occurring at the left and right ends of the sorbent jelly-roll as oriented in Fig. 22. Testing verified that the previous insulation, alumina paper, was not thick enough to prevent flow between the edge of the jelly roll and the ceramic plate. Present models focus on matching the temperature and water concentrations of the experiments.

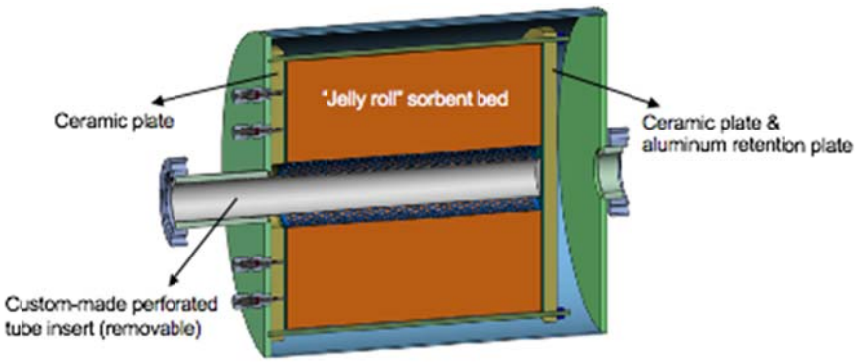

Figure 22. Internal cross-section view of the Microlith-based radial flow adsorber design concept.

The full-scale H_2O jelly-roll has 100 layer pairs of alternating sorbent and wire mesh, with 10 layers of sorbent-only mesh on the exterior of the roll. Ambient temperature air with a water concentration of 0.32 mol m^{-3} flows through the jelly-roll at 566 slpm.

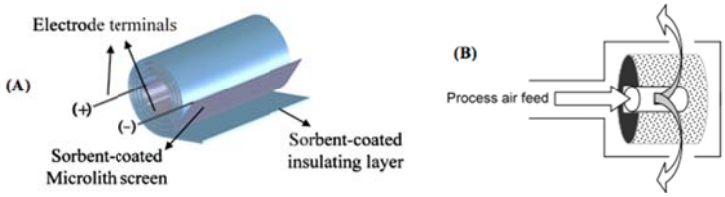

Figure 23. Simplified microlith-based radial flow adsorber design consisting of a "jelly-roll" coil of sorbent-coated microlith screens and sorbent-coated insulating meshes (A) in a radial flow configuration (B).

E. Models

Except for assuming cylindrical axisymmetry, the model module details are very similar to that used for the IBD, simultaneously solving for temperature, concentration, and loading. Air properties at 20 ºC and 1.002 bar were assumed for the input and sorbent volumes. Porosity was assumed to be a constant 0.5. Boundary conditions at the inlet were designated as standard volumetric flow rate and at the outlet as outflow with no viscous stress. The inlet volumetric flow rate, with a dry bulb temperature of 21.6 ºC and a dew point of -9.6 ºC, was held constant at 566 slpm. The LDF constant, $\mathbf{k_m}$, and axial dispersion, $\mathbf{D_i}$, were held constant, while the permeability, which is not a well defined *a priori* value for a wire-coated sorbent bed, was varied in order to match test measurements of overall pressure drop. The model geometry and mesh are further illustrated in Fig. 24.

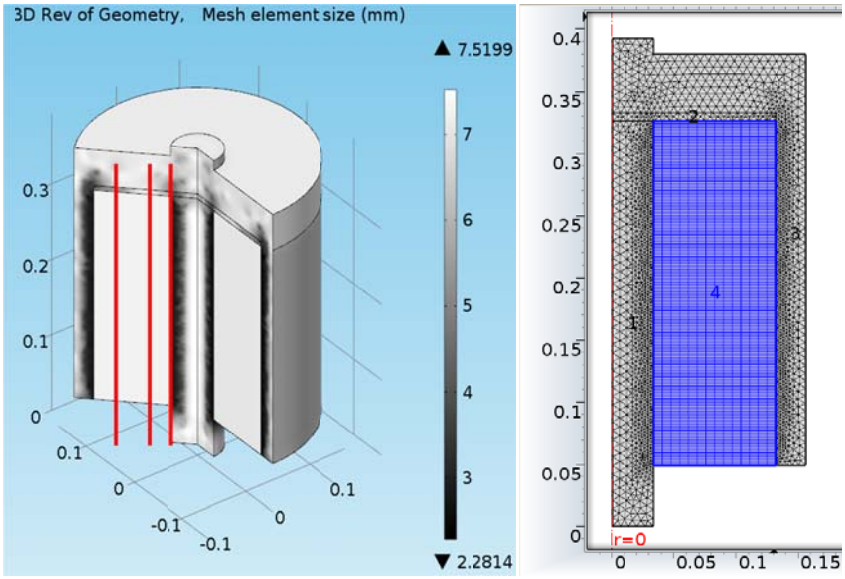

Figure 24. Geometry (left) and mesh (right) of the COMSOL model of the microlith-based radial flow adsorber design.

F. Results and Discussion

A value of 5.79e-10 m^2 was used for the permeability. The breakthrough of water concentration is illustrated in Fig. 25 at the supply inlet and at the nine axial locations between the red marks in Fig. 24. Although there is an axial gradient, as shown in Fig. 26 (where flow is from the top), with breakthrough occurring sooner closer to the inlet, the integrated results show that bulk breakthrough takes over 20 hrs at this flow rate and inlet dew point. One of the poorly known inputs to the model, however, is the thermal coupling between the jelly-roll material and the housing. In a companion model, the heat transfer coefficient was assumed to be a moderate 100 W m^{-2} K^{-1}. As shown in Fig. 27, although the breakthrough timing can be moderately well matched, the resulting simulated peak temperatures vary from that in the experiment. Note the thermo-couples are several mm from locations assumed in the simulation and should be adjusted in future modeling.

This model will provide a means for optimization of cyclic parameters for this particular hardware, and allow for design optimization studies for new Microlith designs.

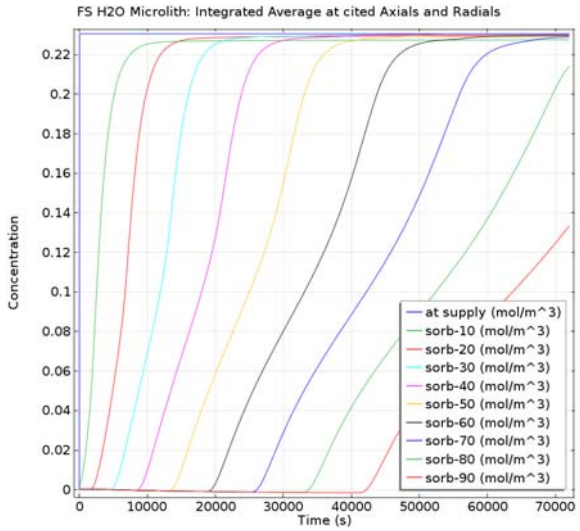

Figure 25. Axially averaged model Concentration results at the three red radial locations drawn in Fig. 24.

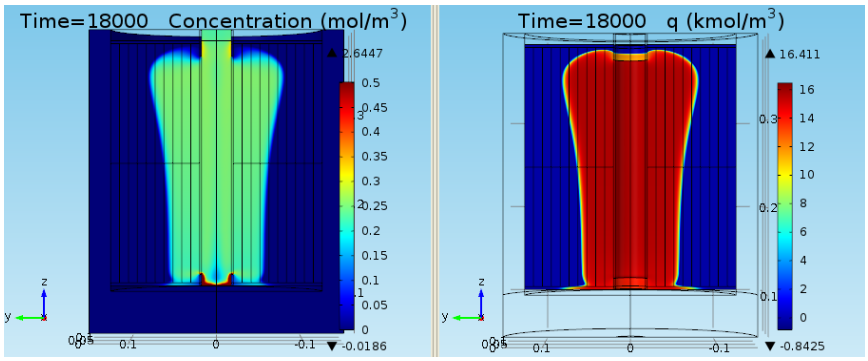

Figure 26. Concentration (left) and loading (right) of the COMSOL model of the microlith-based radial flow adsorber design after 18000 s, with flow from the top.

V. VSA POC

G. Description

A Proof of Concept (POC) vacuum swing adsorption (VSA) canister has been designed, with the goal to maintain a respirable atmosphere through both carbon dioxide removal and humidity control for a portable life support system within a single sorbent bed. The objective of the VSA POC simulation effort is to develop and correlate a baseline mathematical model of such a a canister loaded with Zeolite 13X. Previous vacuum desorption efforts have used analogies to atmospheric pressure models with varying degrees of success. Since the VSA POC will be used to maintain both humidity and carbon dioxide levels within

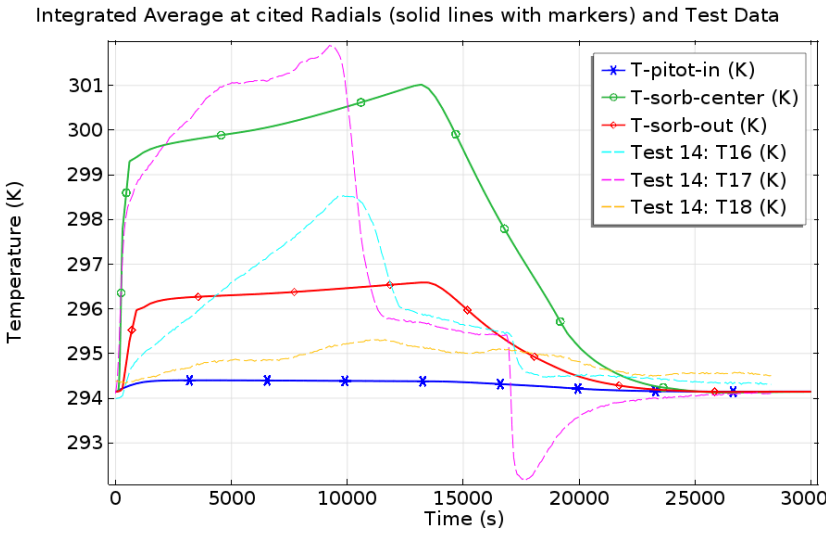

Figure 27. Axially integrated temperatures from the model (solid curves) and measured values from the experiment (dashed curves).

acceptable crew limits, new and/or different physics must be included to account for multi-species adsorption/desorption, potential transitional or free molecular flow and compressibility effects as the sorbent beds are evacuated from atmospheric pressure to vacuum. This will provide a path to higher fidelity multi-dimensional models.

The VSA POC canister is shown in Fig. 31. The canister is 3" in diameter and approximately 8" long, allowing for variable sorbent bed loads from 1" to 8" in length. In adsorption mode the gas flows through the canister (from left to right in the side view) and is evacuated from the left with the aid of external valving. A retaining porous plate along with the internals of the unloaded canister is visible in the isometric view. Just as for the IBD, fine mesh screens (not shown) behind the porous plates are used to hold the sorbent pellets within the bed.

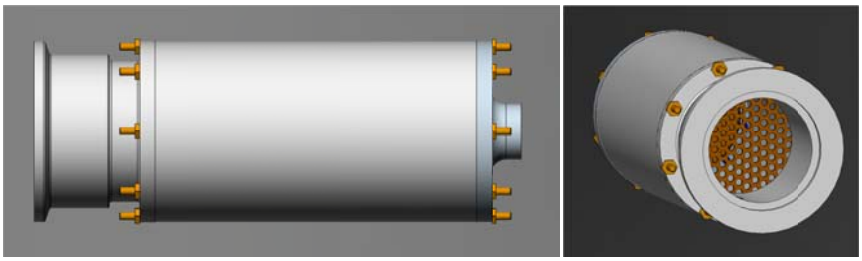

Figure 31. Side (left) and isometric (right) view of the VSA POC canister.

H. Model

The VSA POC canister is modeled with a one dimensional discretization in COMSOL Multi-physics® utilizing separate modules for Concentrated Species (Conservation of Mass), Heat Transfer (Conservation of Energy), General Form PDE 1 (for pellet loading), and General Form PDE 2 (Continuity and Momentum). The multi-component adsorption physics is represented through internal variables and symbols and bed cycling is implemented via Matlab® scripting.

A representative bed model is shown in Fig. 32 and is defined by a cross sectional area, A, a void fraction, ε, and a superficial velocity, V_s. An infinitesimal slice of the bed, Δx, is shown from which to construct mass and energy balances for the flow through the bed. For the mass fraction of an individual species, *i*, represented by ω_i, the advection of the species through the bed, with a source term to represent the adsorption/desorption of the species from the sorbent, can be shown to be given by:

$$\frac{\partial(\rho\omega_i)}{\partial t} + \frac{V_s}{\epsilon}\frac{\partial(\rho\omega_i)}{\partial x} - \frac{\rho D_i}{\epsilon}\frac{\partial^2\omega_i}{\partial x^2} = \frac{\partial q_i}{\partial t}\rho_s\frac{(1-\epsilon)}{\epsilon} \quad (10).$$

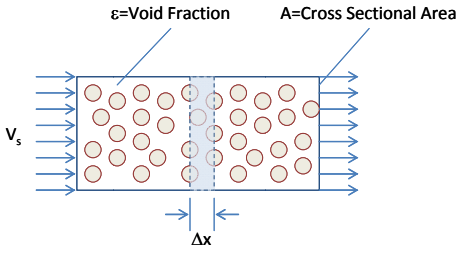

Figure 32. 1-D Bed model representation.

The rate of adsorption or desorption is expressed as the product between a defined Linear Driving Force (LDF) and the difference between the current and equilibrium bed loadings as shown in Eq. (6) above, though here this is solved for each constituent, *i*. The component equilibrium bed loading, $\mathbf{q_i^*}$, is described in the following section.

The multi-component adsorption model for H_2O, CO_2, N_2 and O_2 is described by the equilibrium bed loading (for a single component *i*) defined by Eq. (11) below. A modified form of the Toth equation is used to determine the equilibrium bed loading of the multiple components as a function of the constituent partial pressure and temperature; this depends upon empirical Toth parameters as measured and formulated by Ritter (2012). The Toth implementation is defined by three equations, where the Toth equation parameters $\mathbf{m_{Oi}}$, $\mathbf{b_{Oi}}$, $\mathbf{m_{Ti}}$, $\mathbf{B_i}$ and $\mathbf{q_{si}}$ are predefined to calculate the Toth variables $\mathbf{m_i}$ and $\mathbf{b_i}$, as well as the equilibrium bed loading from the local pressure and temperature (**P** and **T**). The summation is over all components in the model and $\mathbf{P_i}$ represents the partial pressure of the individual constituent. The temperature dependent variables $\mathbf{m_i}$ and $\mathbf{b_i}$ are described in Eqs. (12) and (13). All input parameters are contained in Table 1.

$$q_i^* = \frac{b_i P_i q_{si}}{\left[1 + \left(\sum_j b_j P_j\right)^{m_i}\right]^{\left(\frac{1}{m_i}\right)}} \quad (11)$$

$$b_i = b_{oi}\exp\left(\frac{B_i}{T}\right) \quad (12)$$

$$\mathbf{m_i = m_{oi} + \left(\frac{m_{Ti}}{T}\right)} \quad (13)$$

Table 1. Competitive Adsorption Parameters for 13X

13X	q_{si} (mol/kg)	b_{oi} (1/kPa)	B_i (K)	m_{oi}	m_{Ti} (K)
H_2O	15.0622	2.4100E-07	6852.0	0.390	-4.20
CO_2	5.7117	1.0170E-08	5810.2	0.555	-64.65
N_2	2.2500	6.9467E-07	2219.9	1.000	0.00
O_2	3.9452	1.0754E-06	1683.1	5.200	-1216.33

Two general form PDE modules were used within COMSOL to represent overall continuity and conservation of momentum. Using the ideal gas law, the momentum solver was modified from a traditional density and velocity based conservative form to use pressure and velocity as independent variables for easy integration with the remaining physics in the overall COMSOL model. The transient momentum PDE form in COMSOL was derived from the Ergun relationship with a time dependent term added to include the gas acceleration.

In order to assess the impact of radiation heat transfer in a packed bed, a simple thermal model, constrained within the shape of a cube with reflective sides and a top and bottom surface set to a boundary temperature, was constructed as shown in Fig. 33. The cube (20mm on a side) was filled with passive spheres (2.67 mm in diameter) in a compact face centered cubic arrangement. The heat transfer was predicted via ray tracing and thermal network solution to estimate an effective thermal conductivity through the medium via radiation. The pellets were considered to be highly absorptive in the infrared spectrum and internal conduction was not considered

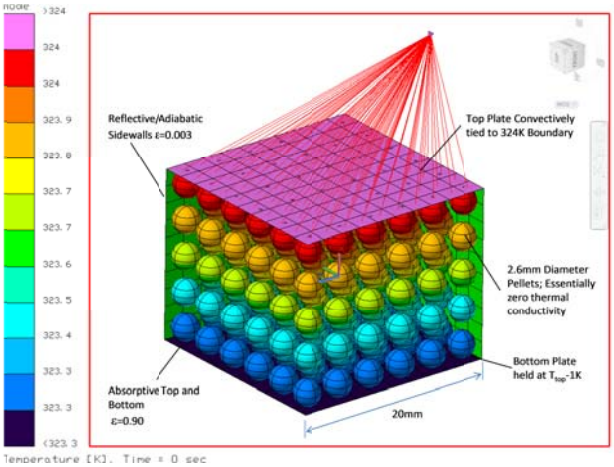

Figure 33. Radiation heat transfer in a packed bed.

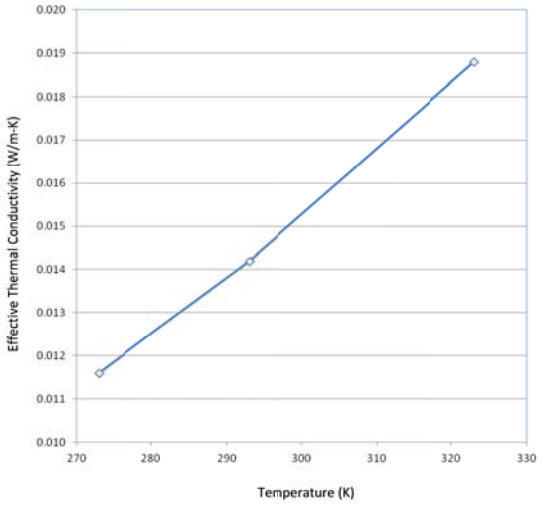

Figure 34. Thermal Conductivity due to Radiation Heat Transfer in a Packed Bed.

Results provided in Fig. 34 show an effective thermal conductivity approaching 0.02 W m^{-1} K^{-1} at warmer bed temperatures. This would be very similar to the thermal conductivity of air at standard conditions. The thermal conductivity prediction (due to radiation) could be a very significant heat transfer mode under evacuated bed conditions during vacuum desorption.

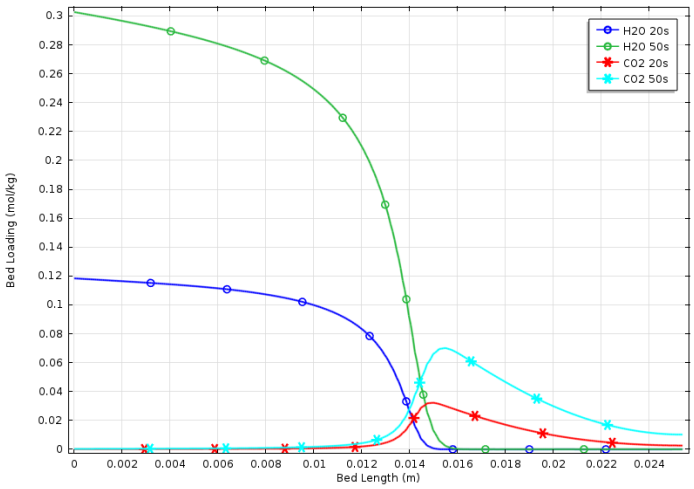

Figure 35. Bed loading vs distance (1") at 50 s during the adsorption half cycle.

A simulation was conducted for a VSA POC bed measuring 1 inch in length filled with 2.67 mm diameter Zeolite 13X pellets. The bed was initially saturated with N_2 at a total pressure of 101325 Pa (1 atmosphere) and temperature of 293.15K. The initial mass fractions of the constituents (H_2O, CO_2, O_2 and N_2) in the gas at the inlet were W_{H2O}= 0.011 (corresponding to a 60°F dew point), W_{CO2}=0.006, W_{O2}=0.283 and W_{N2}=0.7.

The adsorption/desorption half cycle was 50 seconds for the 1 inch bed. During adsorption, the momentum solver is disabled since both pressure and the superficial velocity are defined. The inlet superficial velocity and throughout the bed during adsorption was 0.1 m/s.

Fig. 35 is from an adsorption half cycle. Bed loadings for H_2O and CO_2 at 20 seconds and 50 second are shown. The H_2O and CO_2 concentrations increase as time progresses and it also shows the competitive effects that H_2O has with CO_2 in a Zeolite 13X.

At the end of the adsorption half cycle the momentum solver is enabled to begin the desorption half cycle. To simulate the evacuation of gas from atmospheric conditions to a partial vacuum, the pressure is ramped down from 101325 Pa to 10.13 Pa over one second at the open end of the domain while the other is end is closed off.

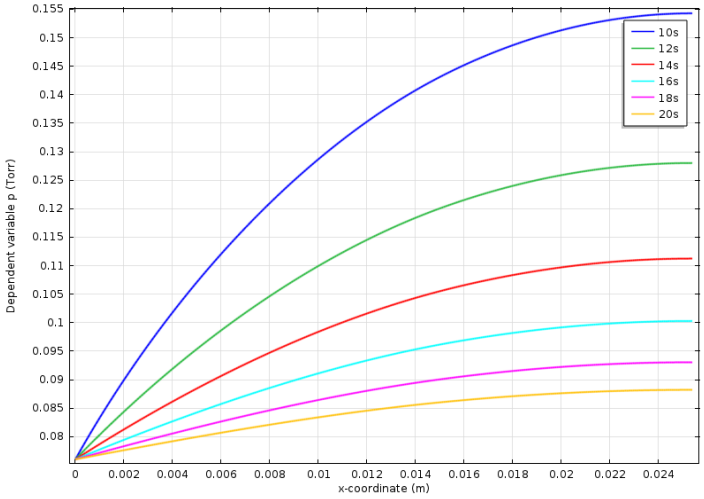

Figure 36. Pressure Blow-down.

The blow-down simulation of the VSA POC bed model is provided in Fig. 36 which shows the pressure distribution throughout the bed for the specified times ranging from 10 to 20 seconds after vacuum desorption is initiated.

I. Results and Discussion

This specific model only went through one adsorption/desorption full cycle. Fig. 37 shows the end of the adsorption and desorption cycle. It shows H_2O and CO_2 concentrations after adsorption but no change in H_2O and very little CO_2 removal after desorption. For this specific case, the pressure in the bed would have to drop significantly lower in order to see H_2O removed since bed loading is a function of pressure and temperature based on the Competitive Langmuir Isotherm described above.

The adsorption/desorption process will be cycled using MATLAB scripting which enables the user to control the number of cycles and cycle length. With the increase in cycles, the bed should reach saturation of H_2O throughout the bed. The H_2O concentration wave would eventually push and remove the CO_2 from the bed due to its competitive effects. At higher H_2O concentrations, desorption would be more significant since H_2O loading drops at 10 Pa after a desorption half cycle.

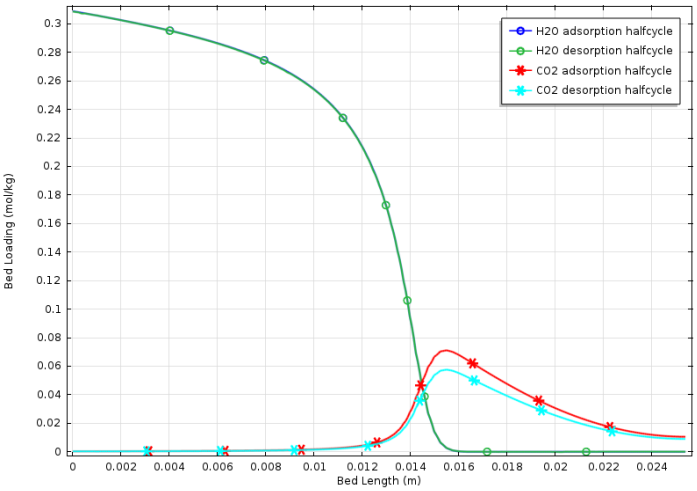

Figure 37. H_2O and CO_2 bed loading vs distance (1") after 1 desorb and adsorb cycle, each 50s long.

VI. Conclusion

The need for atmosphere revitalization systems that are optimized with respect to performance, resources, and is necessitated by the aggressive new missions planned by NASA. With NASA budgets remaining flat, innovative approaches to new system development are required. This paper presents such an approach for the ARREM project, where testing is supplemented with modeling and simulation to reduce costs and optimize hardware designs. In this paper, we have discussed the optimization of heat transfer for development of a Isothermal Bulk Desiccant (IBD) and the application of the fixed bed model in 3D to simulate a cyclic IBD sub-scale test. Studies of the Microlith® Adsorber flow pattern have been used to troubleshoot performance problems and to obtain a successful solution to the flow. Finally, the groundwork has been laid for a VSA POC test by developing the appropriate, simplified vacuum system equations and verifying them against a detailed 3D multiphysics simulation.

The efforts represented here will be continued to support the design of Atmosphere Revitalization systems under the ARREM project. These modeling and simulation efforts are expected to provide design guidance, system optimization, and troubleshooting capabilities for atmosphere revitalization systems being considered for use in future exploration vehiclesconclusion section is not required, though it is preferred.

References

1 **NASA**. Human Exploration & Operations (HEO). 2012).

2 **Mohamadinejad, H., Knox, J.C. and Smith, J.E.** Experimental and Numerical Investigation of Adsorption/Desorption in Packed Sorption Beds under Ideal and Nonideal Flows. *SEPARATION SCIENCE AND TECHNOLOGY*, 2000, **35**(1), 1-22.

3 **COMSOL**. COMSOL Multiphysics®. 2009).

4 **Perry, J., Howard, D.F., Knox, J.C. and Junaedi, C.** Engineered Structured Sorbents for the Adsorption of Carbon Dioxide and Water Vapor from Manned Spacecraft Atmospheres: Applications and Testing 2008/2009. *International Conference on Environmental Systems* (SAE, Savannah, GA, 2009).

5 **Corporation, E.A.** Duocel® Aluminum Foam.

6 **Fares, E. and Shroder, W.** A Differential Equation for Approximate Wall Distance. *Intl. J. Num. Meth. Fld*, 2002, **39**, 743-762.

7 **Barenblatt, B.I., Zheltov, I.P. and Kochina, I.N.** Basic concepts in the theory of seepage of homogeneous liquids in fissured rocks. *J. Appl . Math. Mech.*, 1960, **PMM 24**, 1286-1303.